Measurements of Absolute Electron Capture Cross Sections in He^{2+} -He and Ne^{8+} -O_2, N_2, CH_4 Collisions

Pu-fang Ma,[1,2] Jia-rong Wang,[1,2] Zi-xiao Zhang,[1] Tian-ming Meng,[1,2] Zi-han Xia,[1,2] Bai-hui Ren,[1,2] Long Wei,[1,2] Ke Yao,[1,2] Jun Xiao,[1,2] Ya-ming Zou,[1,2] Bing-sheng Tu,[1,2,*] and Bao-ren Wei[1,2,†]

Affiliations:

[1]Institute of Modern Physics, Department of Nuclear Science and Technology, Fudan University, Shanghai 200433, China

[2]Key Laboratory of Nuclear Physics and Ion-Beam Application (MOE), Fudan University, Shanghai 200433, China

[*]Bingsheng Tu. *E-mail address:* bingshengtu@fudan.edu.cn

[†]Baoren Wei. *E-mail address:* brwei@fudan.edu.cn

Abstract: The total absolute cross sections of single- and double-electron capture (SEC and DEC) in the collisions of He^{2+} with He and Ne^{8+} with O_2, N_2, and CH_4 were studied in the energy ranges 3.5 to 50 keV/u and 2.8 to 40 keV/u, respectively. Through a deep analysis of the experimental systematic uncertainties in the measurement procedure and data evaluation, the error in the experimental results of the SEC cross sections is less than 9%. Within the uncertainties, the present results of the He^{2+} -He collision show good consistency with previous measurements, validating the experimental system and paving the way for precise measurements of EC cross sections for a variety of ions and neutral gases. The present measurements allow for a test of EC theory and provide crucial EC cross section data for the establishment of plasma models in fusion research and astrophysical X-ray studies.

Key words: highly charged ions; cross section; electron capture; charge exchange

1 Introduction

In recent decades, the collisions between highly charged ions (HCIs) and neutral atoms or molecules have become an extremely active area of research [1-3]. Studies on the collision process of HCIs not only contribute to the understanding of fundamental properties such as atomic structure and decay [4] but can also be used to explain the many-body dynamics of electron-correlation effects and the interactions between ions and electrons, atoms, or molecules [5]. Additionally, it is of great relevance in various research fields, such as astrophysics, controlled thermonuclear fusion, materials science, heavy ion physics, ion accelerator technology, and laser research [6]. EC or charge exchange (CE), which predominates all other types of inelastic collisions at impact energies of a few keV/u, affects the ionization balance and results in spectral line emissions in astrophysical

regions or fusion devices [7,8]. It is one of the most significant processes that occur during collisions between HCIs and atomic or molecular species. For example, HCIs are most likely to proceed to highly excited states after collisions with atomic targets. Line radiation from the excited states of impurity ions resulting from EC is known to be one of the major sources of energy loss in magnetic confinement fusion plasmas [9] and is highly valuable for determining ion densities, measuring ion temperatures, and plasma rotation [10].

From an astrophysical perspective, the EC process has been recognized as the primary source of X-ray emission for HCIs interacting with cometary neutral species [11,12], circumstellar neutral clouds [13], and the outer heliosphere, such as supernova remnants [14] and starburst galaxies [15]. Essential to these applications is the measurement of EC cross sections in collisions between HCIs and neutral gases. Reliable knowledge of cross sections is important for modeling various collision processes [16-18]. Some advanced models have been constructed by utilizing various datasets of EC cross sections to improve the accuracy of predictions of the abundance of elements, ion or electron temperature, ionization age, and ionization stage within the heliosphere, planetary exospheres, and supernova remnants. Additionally, these models can provide insights into the outflow structures in galaxies [19,20]. In 2007, Bodewits et al. [21] developed a charge-exchange emission (CXE) model that included H- and He-like carbon, nitrogen, and oxygen ions using a data compilation of the cross section. Their analysis demonstrated that the cometary X-ray spectra reflect the characteristics of the comet, solar wind, and observational conditions. In 2021, Liang et al. [22] considered the DEC process in the CE model and investigated the X-ray emissions of highly charged carbon, nitrogen, oxygen, and neon ions from solar wind using experimental EC cross section data as input. Therefore, accurate EC cross section data are important parameters for these theoretical models, which can improve the reliability of X-ray emission models to realistically simulate these environments, line ratios, and spectra [20].

Widespread attention has been paid to EC cross section measurements, which provide crucial data for establishing plasma models in fusion research and astrophysical X-ray studies. In 2006, applying the initial growth rate method, SEC and DEC cross sections of He^{2+} ions in collisions with N_2, O_2, CO, and CO_2 molecules were measured within an energy range of 0.20 to 2.70 keV/u [23]. Similar measurements have also been carried out for H_2 molecules within an energy range of 0.13 to

0.40 keV/u. In the experiment, He^{2+} ions extracted from a Nier-type electron impact ion source collided with the target gas molecules in a collision cell. The SEC and DEC were derived by measuring the charge fractions of the primary and product helium ions and atoms from the charge spectrum recorded on a pulse-height analyzer. The total experimental uncertainties for the absolute cross sections ranged from 14% to 18%. In 2007, da Silva et al. [24] measured the SEC and DEC cross sections for He^{2+} ions colliding with O_2, H_2, and D_2 at impact energies below 2 keV/u, with experimental uncertainties below 20%. Their technique combined the collection of slow-product ions with primary ion beam attenuation and stopping in a differentially pumped target gas chamber. In this study, the EC cross sections were obtained by measuring the primary ion current without attenuation and the separated current of singly charged He^{+} ions produced during collisions. In 2018, Moradmand et al. [25] reported the total absolute cross sections of SEC and DEC for $Si^{(7\text{-}10)+}$ ions colliding with He and H_2 targets in the energy range of 0.88-2.50 keV/u. In the experiment, the currents were measured for each CE step using a retarding-potential analyzer placed at the end of the gas cell to calculate the EC cross section. The total experimental error ranges from 8% to 11%. In 2019, time-of-flight mass spectroscopy was employed to study the absolute cross sections of SEC for the interactions between CO molecules and He^{2+}, C^{2+}, N^{2+}, and O^{2+} ions [26]. The SEC cross sections were determined by analyzing the mass spectra generated by processes that produced either a molecular ion or a single charged atomic fragment. Measurements are made in the energy range of 6.4 to 36.4 keV with an error of approximately 10%. Overall, advances in experimental facilities and techniques have allowed accurate measurements of EC cross sections, resulting in experimental SEC cross sections with an error of less than 10% in the best case. At present, measurements of the EC cross section are usually limited to a narrow energy range below a few keV/u, and there is still an increasing demand for experimental data over a wide energy range for spectral modeling.

To accurately measure the EC cross sections over a wide energy range, a highly charged ion collision platform was constructed at Fudan University in Shanghai [27]. This article introduces the experimental setup and examines the sources of systematic uncertainties arising from both the experimental apparatus and measurement procedures in detail. Several measures have been adopted to improve the precision of the EC cross section measurement, including numerical calculations aimed at correcting the effective collision length of the gas cell, calibrating the detector

homogeneity, and assessing the measurement data using a gross error analysis method. Following these improvements, the total absolute cross sections of SEC and DEC were accurately measured for $^{4}He^{2+}$ -He as well as $^{20}Ne^{8+}$ -O_2, N_2, and CH_4 collisions from $5q$ keV to $100q$ keV (q is the charge state of ions), and the experimental error of the absolute SEC cross sections was reduced to below 9%. Furthermore, the collision systems between Ne^{8+} ions and O_2, N_2, and CH_4 were theoretically analyzed using a classical over-barrier model (OBM).

2 Experimental Method

The present experiment was carried out with a 150 kV highly charged ion collision platform at Fudan University to measure the absolute cross sections of EC in the collision of HCIs beams with neutral gas targets. The main experimental apparatus was introduced in our previous work [28] and included an electron cyclotron resonance (ECR) ion source, a magnetic analyzer, a gas cell, electric deflectors, and a detector, as shown in Fig.1. The difference in the setup was the replacement of a series of channel electron multipliers (CEMs) by a position-sensitive detector (PSD) in the present experiment [29]. The PSD consists of two pieces of 80 mm diameter Microchannel Plate (MCP) and a Delay-Line Anode. Two pieces of MCP were placed in a chevron structure, and the dead time for multihit detection was approximately 40 ns. A brief introduction of the experiment is provided below.

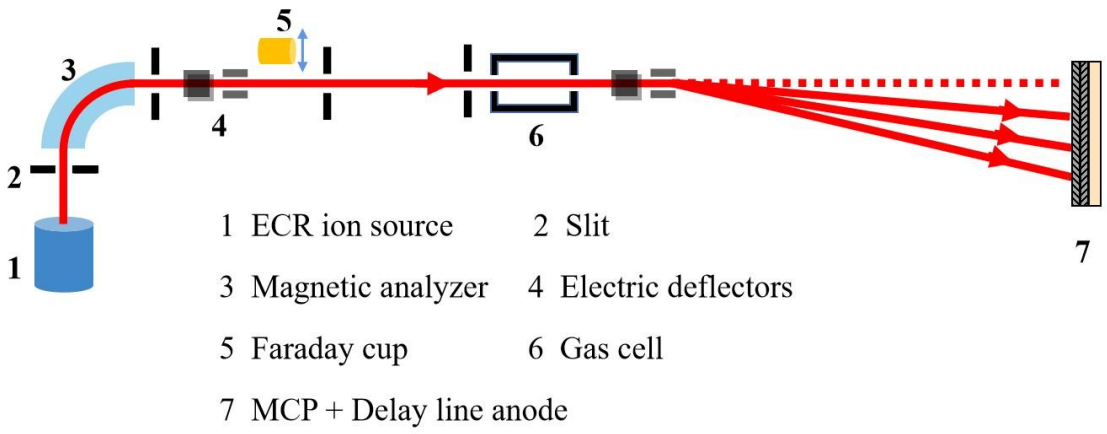

Fig.1 Schematic drawing of the experimental apparatus.

HCI beams with different charge states are produced by an ECR ion source that is operated while floating in a high-voltage state, and the kinetic energy of the ion beam can be tuned from $5q$ keV to $100q$ keV. An ion beam with an appropriate charge state was selected by passing it through a

90° magnetic analyzer and then collimating it using a set of beam optimization and diagnostic components consisting of slits, electric deflectors, and Faraday cups. The gas target was continuously bombarded by the HCIs as the ion beam passed through the gas cell. The pressure in the gas cell was well-controlled by a needle valve and was typically below 2 Pa, whereas the background pressure in the other chambers on the beamline was below 10^{-6} Pa. In this case, the experimental criteria for a single collision between the ion beam and atomic gas in the gas cell can be achieved, and the possibility of accidental CE processes with background gas along the entire beamline is negligible, which is crucial for the determination of the absolute cross section of the EC using the growth rate method. After the collision in the gas cell, the ions with different charge states are scattered by electric deflectors and eventually hit different positions on the detector at a counting rate of approximately 500–700 per second, in which the dead time of the MCP detector is short enough to record all ions. In previous experiments, a series of CEMs was used to detect scattered ions, which produced an uncertainty caused by the detection efficiency between CEMs for measuring differently charged ions. To eliminate this error, the MCP detector is currently used for detection instead of CEMs because it produces an ion imaging map with uniform detection efficiency for differently charged ions. In combination with a delay-line anode, the MCP detector can provide two-dimensional position information, allowing ions with different charge states to be distinguished. The data were recorded in list mode using a VME system [30].

The growth rate method was used to analyze the EC measurement data [31]. Assuming a single collision condition, the cross section for capturing j electrons by incident ions from the target atoms is

$$\sigma_{q,q-j} = \left(\frac{dF_{q-j}}{d\pi}\right)_{\pi=0}, \tag{1}$$

$$F_{q-j}(\pi) = \sigma_{q,q-j}\pi, \tag{2}$$

where $F_{q-j} = N_{q-j}/N_{total}$ indicates the fraction of ions with charge $q-j$ out of the total number of charged ions, and the gas thickness $\pi = nl = Pl/k_BT$ is the number of target gas molecules in the volume of which the area is 1 cm^2, n is the gas molecule number density, k_B is the Boltzmann constant, T is the thermal temperature of the gas cell in kelvin, P and l are the pressure of the target gas and the effective collision length in the gas cell, respectively. The cross section calculation

formula can be expressed as

$$\sigma_{q.q-j} = \frac{F_{q-j}}{Pl} \cdot k_B T = K \cdot \frac{k_B T}{l}, \quad (3)$$

where the slope K indicates the growth rate of $q-j$ ions as a function of the gas pressure. In the experiment, the statistical counts of different charged ions collected by the detector were recorded, and then F_{q-j} can be calculated. By plotting the fraction of the ion beam in a specific charge state against the gas pressure, the cross section of the EC can be evaluated by determining the slope K of the curve.

3 Data Analysis

3.1 Experimental Uncertainty

Because of the importance of EC cross sections in various fields, careful analysis of the experimental uncertainty that determines the accuracy of EC cross section measurements is required. Several aspects were considered to evaluate the experimental uncertainties in the measurements of the EC cross section, including the accuracy of the determination of the effective collision length in the gas cell; efficiency and homogeneity of the detector; temperature and pressure fluctuations of the gas cell during the measurement procedure; stability of the ion beam in the EC cross section measurement; and statistical uncertainty.

Figure 2a shows the dimensions of the gas cell, which had a length of 60.8 mm and a diameter of 38.1 mm. The cell has an inlet aperture with a diameter of 1 mm and an outlet aperture with a diameter of 3 mm. The target gas diffuses from the gas cell owing to the apertures on both sides, leading to uncertainty in the effective collision length. To better understand the effective collision length, a numerical simulation using the finite element method was performed to analyze the pressure in the gas cell based on a molecular flow model. The calculated results for the target gas pressure along the cell axis are shown in Fig. 2b, where the pressure inside the gas cell is set to 0.02 Pa. The simulation showed the diffusion of the molecular flow through the small apertures at both ends, causing a decrease in pressure near the apertures inside the cell and an increase in pressure outside the gas cell. Because of the small apertures relative to the size of the gas cell and the conical shape design, the diffusion caused by the outflow of gas from the inlet and outlet apertures effectively decreased. The resulting correction factor $\alpha \approx 0.99$ obtained by integrating the pressure

along the cell axis to the boundary of the diffusion model, is smaller than the analytical result $\alpha \approx 1.03$ [32]. The effective length is $l_{eff} \approx 0.99l$, where l is the actual length of the gas cell from entrance to exit. Considering the machining precision of the gas cell and the inaccuracy of the calculation, the error in the effective collision length was conservatively estimated to be 2%, which is a three-fold improvement over our previous EC cross section measurement [28].

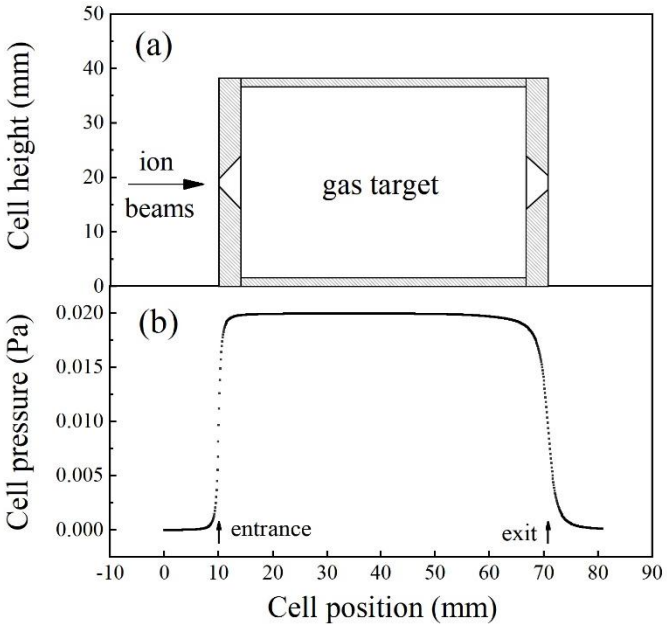

Fig.2 (a) Schematic view of the gas cell and (b) the pressure data along the cylindrical symmetry gas cell axis. The pressure inside the gas cell is set to 0.02 Pa.

Additionally, the detector efficiency of a PSD based on MCP is generally not perfectly homogeneous. Therefore, it is necessary to test the homogeneity of the detector efficiency. Without the injection of incident ions and target gases, the detector area was divided into 90 equally sized rectangular regions, and the background counts generated by the cosmic rays in each region were recorded. The deviation between the distribution of particle numbers in the selected detector area and the average value was calculated as the uniformity coefficient according to Ref. [33]:

$$CU = \left(1 - \frac{\sum_{i=1}^{n} |h_i - \bar{h}|}{\sum_{i=1}^{n} h_i}\right) \times 100, \quad (4)$$

where $\bar{h}$ is the average number of particles in the detection area, h_i is the number of particles in each region, and n is the number of regions. The results show that the detector's uniformity is 94.2%; thus, the inhomogeneity of the detector efficiency is 5.8%. This measurement was repeated two times during the entire experimental period for a reasonable evaluation.

As shown in Eq. (3), the fluctuation in temperature and pressure in the gas cell results in

uncertainty in the measurement of the EC cross section. During the measurements, the temperature and pressure were continuously recorded and their relative fluctuations were below 1% and 3%, respectively. Moreover, the ion beam instability was conservatively estimated to be less than 4% by measuring the intensity of the primary ion beam without a gas target. The statistical errors depend mainly on the experimental setup, including the type of ion beam and target gas, the cross section of the EC, and the gas pressure. Normally, the statistics of the DEC are several times worse than those of the SEC because of the relatively smaller cross section. For instance, after sufficient data acquisition time, the statistical uncertainties of the SEC N_{q-1} and DEC N_{q-2} were 1.8% and 3.3%, respectively, for the Ne^{8+} -O_2 collision.

Table1 Individual and Total Experimental Errors at the 1σ Confidence Level for Ne^{8+} Colliding with O_2

Source of Error	The relative error (%)
Error in temperature	
Temperature difference between chamber and gauge	1
Temperature fluctuation	0.1
Accuracy of temperature	0.1
Error in pressure	
Pressure difference between chamber and pressure gauge	1
Pressure fluctuation	3
Accuracy of pressure gauge	0.25
Error in effective collision length	2
Error in detection efficiency of PSD	5.8
Statistical error	
N_{q-1}	1.8
N_{q-2}	3.3
Stability of beam	4
Total error	
$\sigma_{q,q-1}$	8.2
$\sigma_{q,q-2}$	8.7

A summary of the sources and magnitudes of the experimental errors is presented in Table 1. After a detailed analysis of the effective collision length and a dedicated test for detection efficiency, the uncertainties of SEC and DEC were 8.2% and 8.7%, respectively, for the Ne^{8+} -O_2 collision. Additionally, the experimental uncertainty of the SEC was 8.2% for Ne^{8+} collisions with N_2 and CH_4. The DEC uncertainties for N_2 and CH_4 are 8.8% and 8.6%, respectively.

3.2 Data evaluation

For measurements of the absolute EC cross section, in addition to the systematic uncertainties, the gross error can also significantly affect the accuracy of the experimental measurements. One way to reduce the gross error is to repeat the measurements many times and obtain the mean value. Another method that can be used to identify gross errors and reconcile data is based on Chauvenet's criterion [34,35].

In practice, a measure is rejected if $|y_i - \bar{y}| > \omega \cdot s$, where y_i is the measured value, $\bar{y}$ is the mean value, and s is the standard deviation. ω can be obtained from the criterion table. In general, Chauvenet's criterion is used to identify gross errors in a Gaussian-distributed dataset. To extend this criterion for diagnosing gross errors in the presented EC cross section measurements, it is assumed that the tendency of the measured cross sections can be predicted well by a fitting model. Therefore, the deviations in the experimental data from this model should follow a Gaussian distribution. In this case, Chauvenet's criterion can be applied to identify gross errors in the measurements of the EC cross section.

For instance, the measurements of the SEC cross section of the Ne^{8+} -O_2 collision are shown in Fig. 3. The cross section decreases with a gentle slope as a function of the incident energy, which can be fitted using a quadratic polynomial function (red line in Fig. 3). The standard deviation s of each data point deviating from the fitted model is calculated as follows:

$$s = \sqrt{\frac{\sum_{i,j=1}^{n} (y_i - y_j)^2}{n-1}}, \tag{5}$$

where y_i is the experimental data, and y_j is the value from the fitted line. Then, the confidence bound can be obtained by $y_j \pm s \times \omega$, as shown by the blue dotted line in Fig. 3. Finally, it is simple

to identify the outliers located outside the confidence bound as gross errors. In Fig. 3a, the experimental data with an incident energy of 28.8 keV/u are considered as the gross error; thus, this measurement was repeated. After data reconciliation, the results in Fig. 3b of the SEC cross section satisfy Chauvenet's criterion and show a narrower confidence bound, which also proves that the gross error has been eliminated. It should be noted that the method of extending Chauvenet's criterion in estimating gross errors for EC cross section measurements works if the tendency of the cross sections is smooth and can be simply modeled.

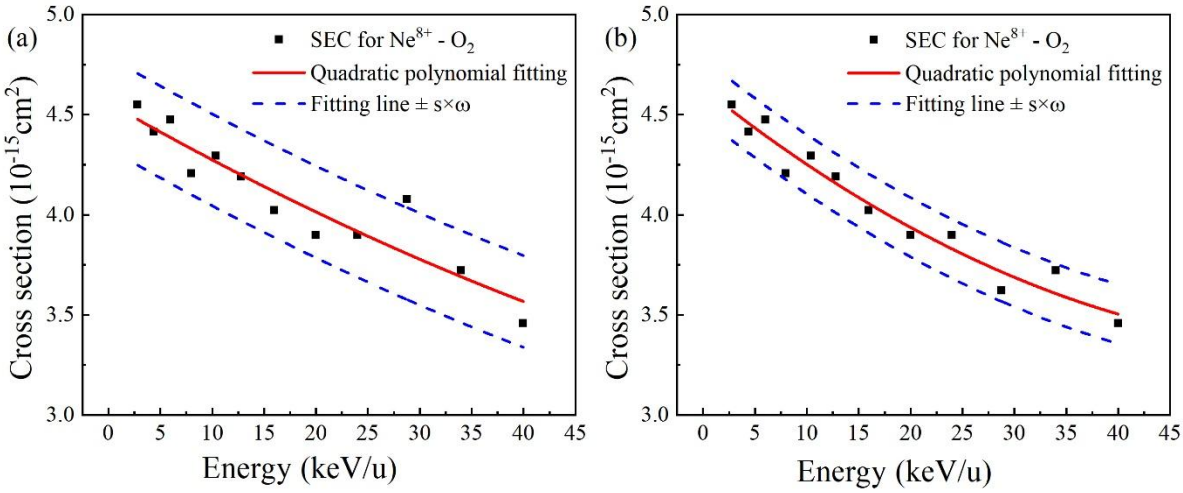

Fig. 3 Data evaluation for SEC cross sections in Ne^{8+} colliding with O_2 between 2.8 and 40 keV/u.

4 Results and Discussion

4.1 $^4He^{2+}$ -He

The significance of EC processes has been demonstrated in both fundamental physics and applied fields [36]. Helium is a fusion reactor product that appears in different ionization states with various relative energies in fusion plasma. The precise measurement of EC cross sections involving ionized helium and molecules is important for plasma modeling and is crucial for the effective removal of helium ash from the divertor region in fusion devices [24]. The measurements of the SEC and DEC absolute cross sections for $^4He^{2+}$ -He were performed with an incident energy of 3.5 to 50 keV/u. The present results of the SEC and DEC cross section measurements of the $^4He^{2+}$ -He collision (black circle) are shown in Fig. 4, with experimental uncertainties of 8.5% and 8.9% for SEC and DEC, respectively.

In Fig. 4a, the SEC cross section increases monotonically from 4.3×10^{-17}cm^2 to 2.9×10^{-16}cm^2 as

the incident energy increases from 3.5 keV/u to 30 keV/u. When the collision energy is above 30 keV/u, the SEC cross section starts to decrease. The present results are consistent with previous experimental SEC cross sections measured by Shah et al. [37] and DuBios et al. [38]. Below 4.65 keV/u, the cross sections of our experiment deviate from the results reported by Mawhorter et al. [32] and Kusakabe et al. [39] but agree with the experimental results of Rudd et al. [40]. The semi-classical close-coupling traveling atomic orbital (AO) theory by Fritsch [41] also displayed good agreement with our measurement of the SEC cross section. Theoretical calculations using a traveling molecular orbital (MO) method within a semiclassical formalism by Kimura [42] are still in good agreement with the present results for energies below 10 keV/u but are approximately 17% lower than the experimental values above 10 keV/u. Figure 4b shows the measurement results of the DEC cross sections for $^4He^{2+}$ -He collisions. The cross sections decrease monotonically as the incident energy increases, which behaves differently from the SEC. The present results show good consistency with the experimental measurements of Berkner et al. [43], Rudd et al. [40], and DuBois et al. [38], as well as the theoretical calculations of Fritsch [41] and Kimura [42] in this energy range.

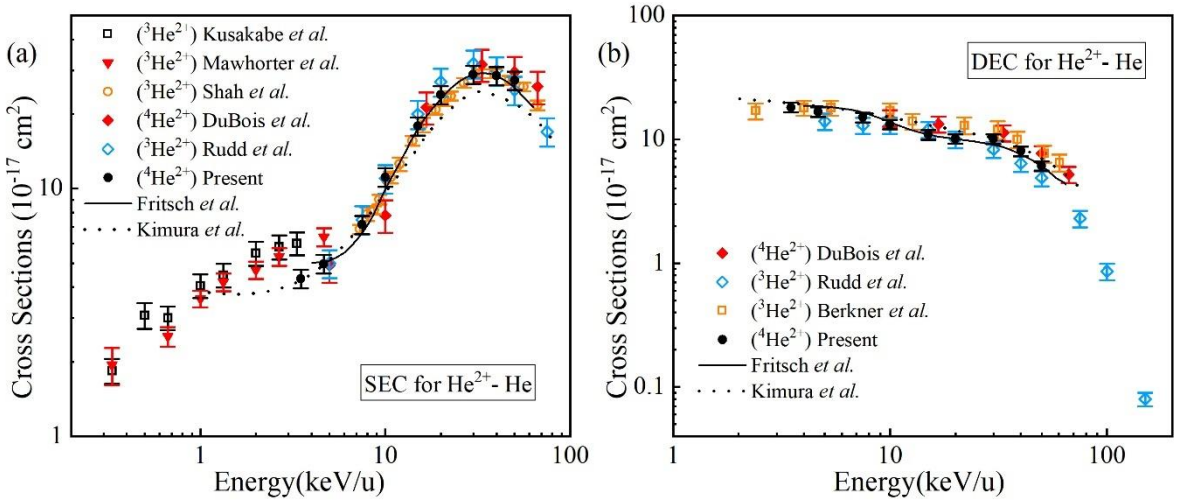

Fig. 4 Measured absolute (a) SEC and (b) DEC cross sections for $^4He^{2+}$ colliding with He.

(a) Experiments: filled black circle (●), current results; hollow blue diamond (◇), results of Rudd et al. [40]; filled red diamond (◆), results of DuBois et al. [39]; hollow orange circle (○), results of Shah et al. [37]; filled red inverted triangle (▼), results of Mawhorter et al. [32]; hollow black square (□), results of Kusakabe et al. [39]. Theories: solid line (—), results of Fritsch. [41]; dotted line (……), results of Kimura. [42]. (b) Experiments: filled black circle (●), current results; filled red diamond (◆), results of DuBois et al. [38]; hollow blue diamond

(◇), results of Rudd et al. [40]; hollow orange square (□), results of Berkner et al. [43]. Theories: solid line (—), results of Fritsch. [41]; dotted line (……), results of Kimura. [42].

In general, the present results are in good agreement with previous experimental results, demonstrating the reliability of the experimental system, which includes the experimental platform operations, collision parameter optimizations, data acquisition systems, and data analysis methods. At low-impact energies, the cross section of the DEC is larger than that of the SEC. A similar result has also been reported for the He^{2+}-He [44] and C^{4+}-He collisions [45]. A possible reason for this is the resonant processes of the DEC explained by Zapukhlyak et al. [46]. To further understand the DEC cross section over the SEC in the low collision energy range, more work is needed from both experiments and theory to explain the physical mechanism.

4.2 $^{20}Ne^{8+}$-O_2, N_2, CH_4

As one of the constituents of the solar wind, it is necessary to estimate the total cross sections of neon ions to simulate ion-neutral collision processes in astrophysical environments and to understand the interactions between the solar wind and the Earth's magnetosphere. Neon ions are also important in the study of fusion reactions and have been used as diagnostic tools to measure plasma temperature and density. The measurement results of the SEC and DEC cross sections for $^{20}Ne^{8+}$ colliding with O_2, N_2, and CH_4 with incident energy from 2.8 to 40 keV/u are shown in Fig. 5 and Table 2. In Fig. 5, the measured absolute cross sections for SEC and DEC both diminish with a gentle slope as the incident energy increases from 2.8 keV/u to 40 keV/u. Qualitatively, the EC cross sections for these targets do not show a typical dependence on the collision energy over the present energy range. The ratios of the DEC to SEC cross sections for the O_2 and N_2 targets were almost constant, with average values of 0.31 and 0.30, respectively, whereas the cross section ratio for the CH_4 target decreases by 21% with increasing collision energy from 0.33 at 2.8 keV/u to 0.26 at 40 keV/u. The experimental results show that for the same collision energy, there is only a slight variation in the absolute SEC cross sections of $^{20}Ne^{8+}$ ions when colliding with different target gases. This is because the capture process depends primarily on the initial binding energies of the electrons in the target. The first ionization energies of N_2, O_2, and CH_4 are 15.6 eV, 12.1 eV, and 12.6 eV, respectively.

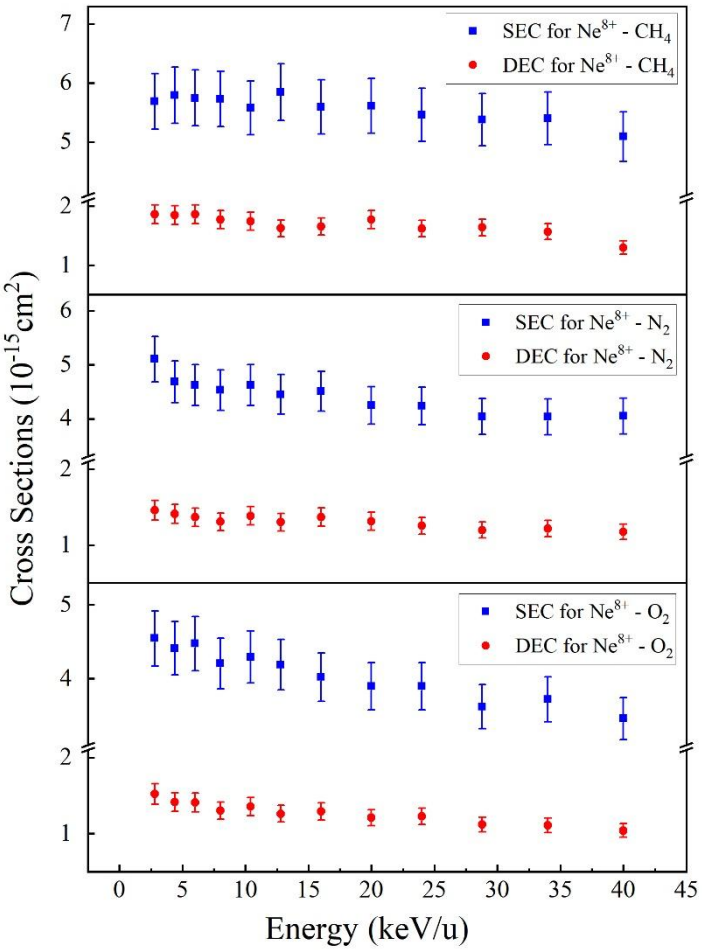

Fig. 5 Measured absolute SEC (filled square ■) and DEC (filled circle ●) cross sections for $^{20}Ne^{8+}$ colliding with CH_4, N_2, and O_2. The errors are given at the 1σ level.

Table2 Absolute Measurements of SEC and DEC Cross Sections for $^{20}Ne^{8+}$ Colliding with N_2, O_2, and CH_4

keV/u	process	N_2	O_2	CH_4
2.8	$\sigma_{q,q-1}$	5.10 ± 0.42	4.55 ± 0.37	5.69 ± 0.47
	$\sigma_{q,q-2}$	1.46 ± 0.13	1.52 ± 0.13	1.86 ± 0.16
4.4	$\sigma_{q,q-1}$	4.68 ± 0.39	4.41 ± 0.36	5.79 ± 0.47
	$\sigma_{q,q-2}$	1.41 ± 0.12	1.42 ± 0.12	1.85 ± 0.16
6.0	$\sigma_{q,q-1}$	4.62 ± 0.38	4.47 ± 0.37	5.75 ± 0.47
	$\sigma_{q,q-2}$	1.37 ± 0.12	1.41 ± 0.12	1.86 ± 0.16
8.0	$\sigma_{q,q-1}$	4.53 ± 0.37	4.21 ± 0.35	5.73 ± 0.47
	$\sigma_{q,q-2}$	1.31 ± 0.11	1.30 ± 0.11	1.78 ± 0.15
10.4	$\sigma_{q,q-1}$	4.62 ± 0.38	4.29 ± 0.35	5.58 ± 0.46
	$\sigma_{q,q-2}$	1.39 ± 0.12	1.36 ± 0.12	1.74 ± 0.15

12.8	$\sigma_{q,q-1}$	4.45 ± 0.37	4.19 ± 0.35	5.85 ± 0.48
	$\sigma_{q,q-2}$	1.30 ± 0.11	1.26 ± 0.11	1.63 ± 0.14
16.0	$\sigma_{q,q-1}$	4.51 ± 0.37	4.02 ± 0.33	5.60 ± 0.46
	$\sigma_{q,q-2}$	1.37 ± 0.12	1.29 ± 0.11	1.66 ± 0.14
20.0	$\sigma_{q,q-1}$	4.25 ± 0.35	3.90 ± 0.32	5.61 ± 0.46
	$\sigma_{q,q-2}$	1.32 ± 0.12	1.21 ± 0.11	1.77 ± 0.15
24.0	$\sigma_{q,q-1}$	4.24 ± 0.35	3.90 ± 0.32	5.46 ± 0.45
	$\sigma_{q,q-2}$	1.25 ± 0.11	1.23 ± 0.11	1.62 ± 0.14
28.8	$\sigma_{q,q-1}$	4.04 ± 0.33	3.62 ± 0.30	5.38 ± 0.44
	$\sigma_{q,q-2}$	1.20 ± 0.11	1.12 ± 0.10	1.64 ± 0.14
34.0	$\sigma_{q,q-1}$	4.03 ± 0.33	3.72 ± 0.31	5.40 ± 0.44
	$\sigma_{q,q-2}$	1.22 ± 0.11	1.11 ± 0.10	1.57 ± 0.14
40.0	$\sigma_{q,q-1}$	4.05 ± 0.33	3.46 ± 0.28	5.09 ± 0.42
	$\sigma_{q,q-2}$	1.18 ± 0.10	1.04 ± 0.09	1.30 ± 0.11

Note. All cross sections are in units of 10^{-15} cm^2, and errors are given at 1σ level.

Currently, there is a relative scarcity of experimental and theoretical studies on collision systems involving $^{20}Ne^{8+}$ ions, atoms, or molecules. To date, experimental SEC cross sections of $^{20}Ne^{8+}$ have only been measured for collisions with He or H_2, as reported by Iwai et al. [47] and Bonnet et al. [48]. The present study reports precise measurements of SEC and DEC cross sections in the keV energy range for $^{20}Ne^{8+}$ -O_2, N_2, and CH_4 collisions. Owing to the lack of available data on these collision systems, the SEC cross sections were evaluated by comparison with those estimated using the classical OBM [49]. According to the model, the SEC cross section is affected by only two factors: the charge state of the incident ion, which is treated as a bare nucleus, and the ionization potential of the target atom, which is treated as a one-electron atom with an appropriate effective charge. The principal quantum n of the captured electron is predicted to be the largest integer satisfying the inequality

$$n \leq q\left[2I_P\left(1+\frac{q-1}{2\sqrt{q}+1}\right)\right]^{-1/2}, \tag{6}$$

where I_P is the ionization potential of the target gas and q=8 is the charge state of Ne^{8+}. The crossing distance R_C for collision systems is then given by

$$R_C = \frac{q-1}{q^2/2n^2 - I_P}, \quad (7)$$

and the resulting SEC cross section in the OBM is obtained from $\sigma_{q,q-1} = \pi {R_C}^2$. The values for n and R_C are calculated using the ionization potential of N_2 (15.6 eV or 0.57 au), O_2 (12.1 eV or 0.44 au), and CH_4 (12.6 eV or 0.46 au) from the NIST database [50]. For the same incident ion charge state and close ionization potential, the capture states n of the different targets were all equal to five. The different calculation results of the SEC cross section determined for N_2, O_2, and CH_4 are 8.6×10^{-15} cm^2, 6.2×10^{-15} cm^2, and 6.5×10^{-15} cm^2, respectively, only from the difference in ionization potential. As a relatively simple theoretical model, the OBM can only estimate the SEC cross sections in magnitude, as it does not consider the ion incident energy and the l state of the captured electron. Other advanced theoretical approaches, such as the classical trajectory Monte Carlo method [51], the quantum-mechanical molecular-orbital close-coupling method [52,53], and the atomic-orbital close-coupling method [54,55], are considered more accurate for dealing with collision processes in multibody problems. Therefore, the present measurements of the EC cross section can provide experimental verification of these theoretical calculations.

5 Conclusion

In conclusion, this study presents improvements in the experimental accuracy of absolute EC cross section measurements from several aspects. The effective collision length in the gas cell was corrected using the finite element method. The uniformity of the detector efficiency was well-calibrated. Additionally, Chauvenet's criterion was extended to diagnose gross errors in the measurements. Based on these improvements, the total absolute cross section measurements of He^{2+} -He and Ne^{8+} -O_2, N_2, and CH_4 were performed on a 150 kV highly charged ion collision platform, and the experimental errors of the SEC cross section were below 9%. Through comparison with previous results of EC cross sections in the He^{2+} -He collision with other groups, we examined the experimental platform, optimized the collision parameters, and assessed the data acquisition system and data analysis method. This demonstrates the capability of performing precise measurements of absolute EC cross sections for various ions and atomic gas targets. Such measurements provide an experimental foundation for validating the theoretical calculations and filling in the gaps in the EC cross section data in the corresponding energy region.

Acknowledgments: This work was supported by the National Key R&D Program of China under Grant No. 2022YFA1602504 and the National Natural Science Foundation of China (Grant No. 12204110 and No. U1832201), and Shanghai Leading Academic Discipline Project (Project No. B107).

References

1. R.D. Cowan, The Theory of Atomic Structure and Spectra (University of California Press, Berkeley, 1981)
2. R.K. Janev, L.P. Presniyakov, V.P. Sevelko, Physics of Highly Charged Ions (Springer, Berlin, 1985)
3. R.K. Janev, D. Reiter, U. Samm, Collision processes in low-temperature hydrogen plasmas (Jülich: Forschungszentrum, Zentralbibliothek, 2003)
4. X. W. Ma, S.F. Zhang, W. Q. Wen et al., Atomic structure and collision dynamics with highly charged ions. Chin. Phys. B. **31**, 093401 (2022). https://doi.org/10.1088/1674-1056/ac8736
5. F. Brouillard, J. W. McGowan, Physics of Ion-ion and Electron-ion Collisions (Springer, New York, 1983)
6. J.D. Gillaspy, Highly charged ions. J. Phys. B: At., Mol. Opt. Phys. **34**, R93 (2001). https://doi.org/10.1088/0953-4075/34/19/201
7. M. Barat, P. Roncin, Multiple electron capture by highly charged ions at keV energies. J. Phys. B: At., Mol. Opt. Phys. **25**, 2205 (1992). https://doi.org/10.1088/0953-4075/25/10/006
8. R.K. Janev, H. Winter, State-selective electron capture in atom-highly charged ion collisions. Phys. Rep. **117**, 265 (1985). https://doi.org/10.1016/0370-1573(85)90118-8
9. P.G. Carolan, B.P. Duval, A.R. Field et al., Charge-exchange-excited line radiation in a tokamak (ASDEX) with neutral-particle-beam injection. Phys. Rev. A. **35**, 3454 (1987). https://doi.org/10.1103/PhysRevA.35.3454
10. R.C. Isler, An overview of charge-exchange spectroscopy as a plasma diagnostic. Plasma Phys. Control. Fusion. **36**, 171 (1994). https://doi.org/10.1088/0741-3335/36/2/001
11. T.E. Cravens, Comet Hyakutake X-ray source: Charge transfer of solar wind heavy ions. Geophys. Res. Lett. **24**, 105 (1997). https://doi.org/10.1029/96GL03780
12. V. Izmodenov, Y. Malama, G. Gloeckler et al., Filtration of interstellar H, O, N atoms through the heliospheric interface: Inferences on local interstellar abundances of the elements. Astron. Astrophys. **414**, L29 (2004). https://doi.org/10.1051/0004-6361:20031697
13. B.T. Draine, D.T. Woods, On the H_2 line emission from NGC 6240 and other starburst galaxies. Astrophys. J. **363**, 464 (1990). https://doi.org/10.1086/169358
14. K. Heng, R.A. Sunyaev, Broad Lyα emission from supernova remnants in young galaxies. Astron. Astrophys. **481**, 117 (2008). https://doi.org/10.1051/0004-6361:20078906
15. B.J. Wargelin, J.J. Drake, Stringent X-ray constraints on mass loss from Proxima Centauri. Astrophys. J. **578**, 503 (2002). https://doi.org/10.1086/342270
16. D.J. Zhao, S. Feng, P.J. Cheng et al., Conceptual design of a $Cs_2LiLaBr_6$ scintillator-based neutron total cross section spectrometer on the back-n beam line at CSNS. Nucl. Sci. Tech. **34**, 3 (2023). https://doi.org/10.1007/s41365-022-01152-5
17. P.H. Chen, H. Wu, Z.X. Yang et al., Prediction of synthesis cross sections of new moscovium isotopes in fusion-evaporation reactions. Nucl. Sci. Tech. **34**, 7 (2023). https://doi.org/10.1007/s41365-022-01157-0
18. J.H. Luo, J.C. Liang, L. Jiang et al., Measurement of $^{134}Xe(n,2n)^{133m,g}Xe$ reaction cross sections in 14-MeV region with detailed uncertainty quantification. Nucl. Sci. Tech. **34**, 4 (2023).

https://doi.org/10.1007/s41365-022-01158-z
19. R.S. Cumbee, P.D. Mullen, D. Lyons et al., Charge exchange X-ray emission due to highly charged ion collisions with H, He, and H_2: line ratios for heliospheric and interstellar applications. Astrophys. J. **852**, 7 (2017). https://doi.org/10.3847/1538-4357/aa99d8
20. K.D. Kuntz, Solar wind charge exchange: an astrophysical nuisance. Astron. Astrophys. Rev. **27**, 1 (2019). https://doi.org/10.1007/s00159-018-0114-0
21. D. Bodewits, D.J. Christian, M. Torney et al., Spectral analysis of the Chandra comet survey. Astron. Astrophys. **469**, 1183 (2007). https://doi.org/10.1051/0004-6361:20077410
22. G.Y. Liang, X.L. Zhu, H.G. Wei et al., Charge-exchange soft X-ray emission of highly charged ions with inclusion of multiple-electron capture. Mon. Not. R. Astron. Soc. **508**, 2194 (2021). https://doi.org/10.1093/mnras/stab2537
23. T. Kusakabe, Y. Miyamoto, M. Kimura et al., Charge-transfer processes in collisions of He^{2+} ions with H_2, N_2, O_2, CO, and CO_2 molecules below 4 keV/u. Phys. Rev. A. **73**, 022706 (2006). https://doi.org/10.1103/PhysRevA.73.022706
24. S.F. da Silva, H.P. Winter, F. Aumayr, Single-and double-electron capture cross sections for slow He^{2+} impact on O_2, H_2, and D_2. Phys. Rev. A. **75**, 042706 (2007). https://doi.org10.1103/PhysRevA.75.042706
25. A. Moradmand, M.O.A. El Ghazaly, D.P. Mahaptra et al., Measurement of Absolute Single and Double Charge Exchange Cross Sections for $Si^{(7-10)+}$ at 0.88–2.50 KeV/u Impacting He and H_2. Astrophys. J., Suppl. Ser. **234**, 14 (2018). https://doi.org/10.3847/1538-4365/aaa02c
26. A.A. Basalaev, V.V. Kuz'michev, M.N. Panov et al., Capture and dissociative capture of a single electron in the process of interaction of doubly charged ions with CO molecules. Tech. Phys. **64**, 1096 (2019). https://doi.org/10.1134/S1063784219080024
27. Y. Zhang, T. Jiang, L. Wei et al., Three-body fragmentation of methane dications produced by slow Ar^{8+}-ion impact. Phys. Rev. A. **97**, 022703 (2018). https://doi.org/10.1103/PhysRevA.97.022703
28. J. Han, L.Wei. B. Wang et al., Measurement of Absolute Single and Double Electron Capture Cross Sections for O^{6+} Ion Collisions with CO_2, CH_4, H_2, and N_2. Astrophys. J., Suppl. Ser. **253**, 6 (2021). https://doi.org/10.3847/1538-4365/abde44
29. X.L. Zhu, X.W. Ma, S. Sha et al., Two-dimension delay-line microchannel plate imaging detector. Nucl. Electron. Detect. Technol. **24**, 253 (2004). (in Chinese) https://doi.org/10.3969/j.issn.0258-0934.2004.03.010
30. X.C. Wang, B.R. Wei, Y. Yang et al., A multi-parameter data acquisition system for the collision research platform at Shanghai EBIT. Nucl. Sci. Tech. **20**, 51 (2009). https://doi.org/10.13538/J.1001-8042/NST.20.51-55
31. H. Tawara, A. Russek, Charge changing processes in hydrogen beams. Rev. Mod. Phys. **45**, 178 (1973). https://doi.org/10.1103/RevModPhys.45.178
32. R.J. Mawhorter, J.B. Greenwood, A. Chutjian et al., Measurement of absolute charge-exchange cross sections for He^{2+} collisions with He and H_2. Phys. Rev. A. **84**, 052714 (2011). https://doi.org/10.1103/PhysRevA.84.052714
33. J.E. Christiansen, Irrigation by sprinkling (University of California Press, Berkeley, 1942)
34. W. Chauvenet, A manual of spherical and practical astronomy (Nabu Press, Carolina, 2011)
35. J.R. Taylor, An Introduction to Error Analysis (University Science Books, California, 1997)
36. X.L. Zhu, X.W. Ma, B. Li et al., Experimental differential investigation of state-selective single electron capture in slow He2+-He collisions. Acta Phys. Sin. **58**, 2077 (2009). (in Chinese) https://doi.org/10.7498/aps.58.2077

37. M.B. Shah, P, McCallion, H,B, Gilbody, Electron capture and ionisation in collisions of slow H^+ and He^{2+} ions with helium. J. Phys. B: At., Mol. Opt. Phys. **22**, 3037 (1989). https://doi.org/10.1088/0953-4075/22/19/018
38. R.D. DuBois, Ionization and charge transfer in He^{2+}–rare-gas collisions. II. Phys. Rev. A. **36**, 2585 (1987). https://doi.org/10.1103/PhysRevA.36.2585
39. T. Kusakabe, H, Yoneda, Y. Mizumoto et al., Charge Transfer Cross Sections of $^3He^{2+}$ Ions in Collisions with He Atoms and H_2 Molecules in the Energy Range of 1∼10 keV. J. Phys. Soc. Jpn. **59**, 1218 (1990). https://doi.org/10.1143/JPSJ.59.1218
40. M.E. Rudd, T.V. Goffe, A. Itoh, Ionization cross sections for 10–300-keV/u and electron-capture cross sections for 5–150-keV/u $^3He^{2+}$ ions in gases. Phys. Rev. A. **32**, 2128 (1985). https://doi.org/10.1103/PhysRevA.32.2128
41. W Fritsch, Theoretical study of electron processes in slow He^{2+}-He collisions. J. Phys. B: At., Mol. Opt. Phys. **27**, 3461 (1994). https://doi.org/10.1088/0953-4075/27/15/021
42. M Kimura, Single- and double-electron capture in He^{2+}+He collisions and single-electron capture in He^++He^+ collisions. J. Phys. B: At., Mol. Opt. Phys. **21**, L19 (1988). https://doi.org/10.1088/0953-4075/21/2/005
43. K.H. Berkner, R.V. Pyle, J.W. Stearns et al., Single- and Double-Electron Capture by 7.2- to 181-keV $^3He^{++}$ Ions in He. Phys. Rev. **166**, 44 (1968). https://doi.org/10.1103/PhysRev.166.44
44. S.F. da Silva, G. Kowarik, F. Aumayr et al., Single and double electron capture by slow He^{2+} from atoms and molecules. J. Phys.: Conf. Ser. **58**, 181 (2007). https://doi.org/10.1088/1742-6596/58/1/036
45. L.L. Yan, Y. Wu, Y.Z. Qu et al., Single-and double-electron-capture processes in the collisions of C^{4+} ions with He. Phys. Rev. A. **88**, 022706 (2013). https://doi.org/10.1103/PhysRevA.88.022706
46. M. Zapukhlyak, T. Kirchner, Projectile angular-differential cross sections for electron transfer processes in ion-helium collisions: Evidence for the applicability of the independent electron model. Phys. Rev. A. **80**, 062705 (2009). https://doi.org/10.1103/PhysRevA.80.062705
47. T. Iwai, Y. Kaneko, M. Kimura et al., Cross sections for one-electron capture by highly stripped ions of B, C, N, O, F, Ne, and S from He below 1 keV/amu. Phys. Rev. A. **26**, 105 (1982). https://doi.org/10.1103/PhysRevA.26.105
48. J.J. Bonnet, A. Fleury, M. Bonnefoy et al., Electron capture into different (nl) states in slow collisions of Ne^{8+} projectiles on He and H_2 targets. J. Phys. B: At. Mol. Phys. **18**, L23 (1985). https://doi.org/10.1088/0022-3700/18/2/003
49. R. Mann, F. Folkmann, H.F. Beyer, Selective electron capture into highly stripped Ne and N target atoms after heavy-ion impact. J. Phys. B: At. Mol. Phys. **14**, 1161 (1981). https://doi.org/10.1088/0022-3700/14/7/012
50. NIST Chemistry Webbook. NIST Standard Reference Database Number 69, https://webbook.nist.gov/chemistry/. Accessed 11 April 2023
51. S. Otranto, R. E. Olson, P. Beiersdorfer, X-ray emission cross sections following charge exchange by multiply charged ions of astrophysical interest. Phys. Rev. A. **73**, 022723 (2006). https://doi.org/10.1103/PhysRevA.73.022723
52. J. G. Wang, P. C. Stancil, A. R. Turner et al., Vibrationally resolved charge transfer of O^{3+} with molecular hydrogen. Phys. Rev. A. **69**, 062702 (2004). https://doi.org/10.1103/PhysRevA.69.062702
53. K. Wang, Y. Z. Qu, C. H. Liu et al., Charge transfer in low-energy collisions of Be^{3+} and B^{4+}

ions with He. Chin. Phys. B. **29**, 093401 (2020). https://doi.org/10.1088/1674-1056/aba276
54. W. Fritsch, C.D. Lin, The semiclassical close-coupling description of atomic collisions: Recent developments and results. Phys. Rep. **202**, 1-97 (1991). https://doi.org/10.1016/0370-1573(91)90008-A
55. M. X. Ma, B. H. Kou, L. Liu et al., Electron capture in collisions of Li^{3+} ions with ground and excited states of Li atoms. Chin. Phys. B. **29**, 013401 (2020). https://doi.org/10.1088/1674-1056/ab577f